Supplemental Information for: "Liquid droplets act as "compass needles" for the stresses in a deformable membrane"

Rafael D. Schulman,[1] René Ledesma-Alonso,[2,3] Thomas Salez,[3,4] Elie Raphaël,[3] and Kari Dalnoki-Veress[1,3,*]

[1]*Department of Physics and Astronomy, McMaster University, 1280 Main St. W, Hamilton, ON, L8S 4M1, Canada.*
[2]*CONACYT - Universidad de Quintana Roo, Boulevar Bahía s/n, Chetumal, 77019 Quintana Roo, México*
[3]*Laboratoire de Physico-Chimie Théorique, UMR CNRS Gulliver 7083, ESPCI Paris, PSL Research University, 75005 Paris, France.*
[4]*Global Station for Soft Matter, Global Institution for Collaborative Research and Education, Hokkaido University, Sapporo, Hokkaido 060-0808, Japan.*

(Dated: February 27, 2017)

SAMPLE PREPARATION

Elastomeric films were prepared from Elastollan TPU 1185A (BASF). Solutions of Elastollan in cyclohexanone (Sigma-Aldrich) were prepared at 3% weight fraction. Upon spincoating these solutions, the Elastollan polymers, which contain hard and soft segments, assemble to form an elastomer with physical crosslinks. The Elastollan solutions were cast onto freshly cleaved mica substrates (Ted Pella Inc.) to produce highly uniform (<5% variation) films with of thickness $h \sim 240$ nm, measured using ellipsometry (Accurion, EP3). These films were subsequently heated at 100°C for 90 min to remove any residual solvent from the elastomer. After annealing, these films were floated onto the surface of an ultrapure water bath (18.2 MΩ·cm, Pall, Cascada, LS) and picked up between two supports to form our sample. In our experiments, the liquid we use is glycerol (Caledon Laboratories Ltd.).

LIQUID CAP AND BULGE PROFILES

As explained in the main text, two droplets are placed on the film: one on each side. The purpose of doing so is to be able to visualize both the liquid-air interface and the bulge when viewing the sample from the y-direction, where the supports obscure our view of the lower side of the film. Sample optical microscopy images of of the two profiles when viewed from the y-direction are shown in Fig. S1. In Fig. S1(a), the solid curve represents the best fit of a circular cap to the liquid-air interface profile, and in Fig. S1(b), the dashed curve represents the best fit of a parabola to the bulge profile. The fits desribe the optical profiles well.

From optical profilometry, we find that the film is always pulled up towards the droplet on the low-tension side. This is seen in Fig.2(b) of the main text, where we observe a positive w on the sides of the droplet along the x-direction. In fact, this small deformation can be visualized in Fig. S1, where the film is seen to be pulled up towards the droplet in (a) and suppressed leading into the bulge in (b).

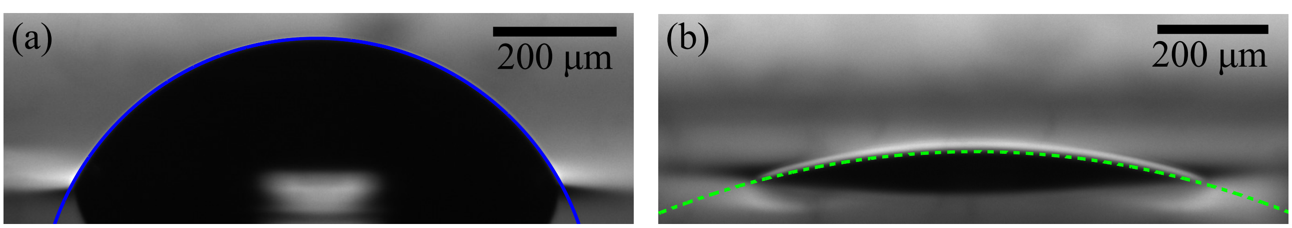

FIG. S1. (a) An optical sideview of a liquid-air interface profile taken from the y-direction, where the solid curve represents the circular cap fit to the profile. (b) An optical sideview of a bulge as seen from the y-direction. The dashed curve corresponds to the parabolic fit to the profile.

As mentioned in the main text, to derive Eq. 1, we assume that the liquid-air interface profile is well described by a circular cap when viewed along any general direction oriented at ϕ to the x-axis. Experimentally, we observe that this assumption is fully reasonable. In Fig. S2, we show a sample profile of a liquid-air interface taken along a sightline corresponding to $\phi = 45°$, where we show the circular fit as a solid curve. As can be seen from this image, as well as any other sightline we have tested, the profile is always well described by a circular cap. Of course, since

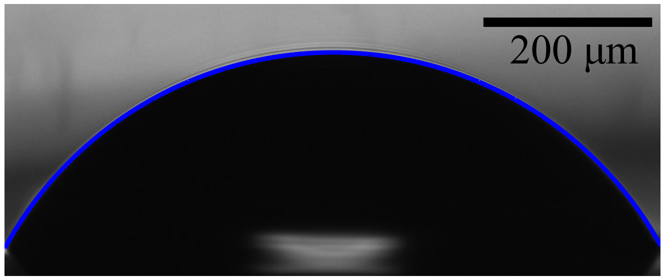

FIG. S2. An optical sideview of the liquid-air interface taken from a sightline oriented at $\phi = 45°$ to the x-axis. The solid curve represents the circular fit to the profile.

the 3D shape of the liquid-air interface is not spherical, the radius of curvature of the circular cap extracted from the profile fits changes along the various sightlines.

TENSION VERIFICATION

Although the technique of using liquid contact angles to measure the tension in deformable membranes has been employed and verified in previous studies [1, 2], we perform an additional validation here. In this experiment, we prepare a film where the tension is isotropic (droplets are completely round within experimental error) and is measured to be $T_{\text{in}}/\gamma = 2.1 \pm 0.1$ using the contact angle technique from the main manuscript. Near the center of the film, we place small dirt particles to act as tracer particles. Next, we stretch the film along the y-axis, and from the tracer particles, the strains induced in the film in both directions are measured to be $e_x = -0.016 \pm 0.006$ and $e_y = 0.195 \pm 0.015$. Next, we perform contact angle measurements once again to determine the tension in this way. We find the change in tension from the initial state to be $\Delta T_{\text{in},y}/\gamma = 6.6 \pm 0.8$ and $\Delta T_{\text{in},x}/\gamma = 2.3 \pm 0.3$. If we suppose the interfacial tensions do not change appreciably upon stretching, the change in tension is purely mechanical.

To derive a theoretical expression for the change in tension upon straining the film, we employ Hooke's law [3]. We assume that there is no stress acting in the z-direction across the film, i.e. $\sigma_z = 0$. We also know that the mechnical tension is related to stress through film thickness $\Delta T = h\Delta\sigma$. Once again, the Δ signifies changes from the reference state of isotropic tension. As such, we may derive simple expressions for the changes in mechanical tension upon stretching:

$$\Delta T_x = \frac{Eh(e_x + \nu e_y)}{1 - \nu^2}, \tag{S1}$$

$$\Delta T_y = \frac{Eh(e_y + \nu e_x)}{1 - \nu^2}, \tag{S2}$$

where ν is the Poisson ratio of the elastomer, which can be assumed to be 0.5 and E is the Young's modulus. Some other quantities of interest to compute are the tension ratio

$$(\Delta T_y/\Delta T_x) = \frac{e_y + \nu e_x}{e_x + \nu e_y}, \tag{S3}$$

since this quantity is independent of the modulus and film thickness, as well as the strain in the vertical direction, representing the fractional change in film thickness upon straining

$$e_z = \frac{\nu}{\nu - 1}(e_x + e_y). \tag{S4}$$

Substituting our measured strain values for the strains into Eq. S3, we find $(\Delta T_y/\Delta T_x) = 2.3 \pm 0.1$. This value is in agreement with the value measured using contact angles $(\Delta T_{\text{in},y}/\Delta T_{\text{in},x}) = 2.9 \pm 0.5$ within experimental error. In addition, as a consistency check, we verify Eq. S4 by measuring the film thickness before and after stretching, to find a change in film thickness of -18.3%, which agrees nicely with the predicted strain of -17.9% from Eq. S4.

To compare the individual values of the tension from contact angles against those from particle tracking, we must know E and γ. We may find values for E in the literature; nevertheless, this introduces error, as E will depend on the details of the sample preparation for a physically cross-linked elastomer. With this caveat in place, we find measured literature values for the Young's modulus of Elastollan be roughly within the range $E = 9 \pm 1.5$ MPa [4–6]. The surface tension of glycerol is $\gamma = 0.063$ N/m [7]. For h in Eqs. S1 and S2, we use the stretched film thickness. As such, our predicted values from particle tracking are $\Delta T_x/\gamma = 3.1 \pm 0.9$ and $\Delta T_y/\gamma = 7 \pm 2$, which compare well with the tensions determined from contact angles.

SHAPE OF THE WETTING REGION PERIMETER

In this section, we outline the arguments used to attain Eq. 1 in the main manuscript. We make some simplifying assumptions to render the problem more tractable. First and foremost, we assume that the shape of the liquid-air interface is a perturbation from a spherical cap. Given this assumption, there are two reasonable approximations which can be made. First, we approximate that any vertical cross-section of the liquid-air interface done along a general line oriented at ϕ (see Fig. 1(b) in the main manuscript) is a circular cap with its own radius of curvature. This assumption is found to be in agreement with the experimental observation that sideview profiles of the liquid-air interface from any such sightlines are well-described by circular caps (example seen in Fig. S2). From the elliptical paraboloid shape of the bulge, which will be discussed in the following section, we know that all cross-sections of the bulge done in the same way are parabolas. Next, if we define ϕ' to be the angle subtended between the x-axis and the in-plane normal of the footprint perimeter, we make the approximation that $\phi' \approx \phi$. Of course, true equality only holds in the limit that the footprint shape is circular ($\epsilon = 1$), but it remains a good approximation for ϵ close to 1.

To begin the derivation, we point out that the vertical distance from the apex of the bulge to the top of the droplet, $h_{\rm tot}$, must be the same for any profile taken from a cross-section along a line oriented at ϕ. For a given ϕ, this height is found as the sum of the liquid cap height $h_{{\rm d},\phi}$ and the bulge height $h_{{\rm b},\phi}$. The height of the liquid cap can be found through a simple circular cap identity $h_{{\rm d},\phi} = r_\phi \tan\theta_{{\rm d},\phi}/2$, where r_ϕ is the footprint radius and $\theta_{{\rm d},\phi}$ is the cap's contact angle, both for this value of ϕ. A similar relationship can be found for the parabola which represents the bulge, $h_{{\rm b},\phi} = \frac{r_\phi}{2}\tan\theta_{{\rm b},\phi}$. Therefore, we can write

$$h_{\rm tot} = r_\phi\Big(\frac{1}{2}\tan\theta_{{\rm b},\phi} + \tan\frac{\theta_{{\rm d},\phi}}{2}\Big). \tag{S5}$$

Our final simplification in this derivation is to assume that $\theta_{\rm b}$ and $\theta_{\rm d}/2$ are small angles, such that $\tan\theta_{\rm b} \approx \theta_{\rm b}$ and $\tan\theta_{\rm d}/2 \approx \theta_{\rm d}/2$. This approximation is reasonable for our experiments where $\theta_{{\rm b},\phi} < 25°$ and $\theta_{{\rm d},\phi}/2 < 33°$, so there is less than 11% error in making this approximation at this point. Generally these assumptions become increasingly more appropriate the smaller $\theta_{\rm Y}$ is. Employing the small-angle limit, we are left with

$$h_{\rm tot} = \frac{r_\phi}{2}\Big(\theta_{{\rm b},\phi} + \theta_{{\rm d},\phi}\Big). \tag{S6}$$

The angle sum $\theta_{{\rm b},\phi} + \theta_{{\rm d},\phi}$ represents the internal angle of the liquid at the contact line, and can be simply predicted using a Neumann construction, as was shown in previous work [2].

$$\theta_{{\rm b},\phi} + \theta_{{\rm d},\phi} = \arccos\Big(\cos\theta_{\rm Y} - \frac{\gamma}{2T_{{\rm in},\phi}}\sin^2\theta_{\rm Y}\Big). \tag{S7}$$

This Neumann construction should be set up normal to the contact line. However, since $\phi' \neq \phi$ as outlined before, the normal line does not pass through the droplet center. Therefore, to simplify the problem, we assume that $\phi' \approx \phi$, which implies that the Neumann construction above represents the internal angle of the liquid for a cross-section taken from the contact line to the droplet center, oriented at an angle ϕ to the x-axis. Thus, noting that $h_{\rm tot}$ in Eq. S6 is just some constant value, we arrive at the final result

$$r_\phi = \frac{C}{\arccos\Big(\cos\theta_{\rm Y} - \frac{\gamma}{2T_{{\rm in},\phi}}\sin^2\theta_{\rm Y}\Big)}, \tag{S8}$$

where $T_{{\rm in},\phi}$ is the total tension in the ϕ direction in the region under the droplet, and C is a constant which simply sets the overall scale of the region. As discussed in the main text, we assume that the deformations produced by the two liquid drops on the film are only perturbative to the pre-tension of the membrane. This assumption was validated in previous study done with isotropic tension [2], but is further supported by the experimental observation that the contact angles remain constant as additional droplets are placed onto the film and also by the tension confirmation using tracer particles described in the previous section. Since we have prepared the film to have a biaxial tension with principal directions in x and y, the tension in any direction ϕ is $T_{\mathrm{in},\phi} = T_{\mathrm{in},x}\cos^2\phi + T_{\mathrm{in},y}\sin^2\phi$ [3].

DERIVATION OF THE BULGE SHAPE

The small-slope out-of-plane deformation of a film $w\,(x, y)$ subjected to a transverse pressure is described by the Föppl-von Kármán equations [8]:

$$D\Delta^2 w - h\nabla \cdot \left(\sigma \cdot \nabla w\right) \; = p, \tag{S9a}$$

$$\nabla \cdot \sigma = 0 \;, \tag{S9b}$$

where p is the transverse pressure distribution, D is the flexural rigidity, h is the film thickness, and σ is the stress tensor. In our system, bending can be neglected, and the first term in Eq. S9a can be ignored. Motivated by experimental observations, we make the simplifying assumption that the deformation of the membrane by the droplet does not notably modify the pre-existing tension. Therefore, the stress in the membrane is the as-prepared biaxial stress which is uniform in the region near the center of the film where the experiment is performed. Since the stress is uniform, Eq. S9b is automatically satisfied, and Eq. S9a can be simplified to:

$$T_{\mathrm{in},x}\frac{\partial^2 w}{\partial x^2} + 2T_{\mathrm{in},xy}\frac{\partial^2 w}{\partial x \partial y} + T_{\mathrm{in},y}\frac{\partial^2 w}{\partial y^2} = -p, \tag{S10}$$

where we have used the general relation that tension is stress multiplied by film thickness. Since the film is prepared with a biaxial tension in which the principal directions are aligned with x and y, it implies that $T_{\mathrm{in},xy} = 0$, thus we are left with

$$T_{\mathrm{in},x}\frac{\partial^2 w}{\partial x^2} + T_{\mathrm{in},y}\frac{\partial^2 w}{\partial y^2} = -p\,(x, y) \;\;, \tag{S11}$$

Since there is no flow within the liquid, the droplet must contain a uniform pressure, so p is a constant value in our case and given by the Laplace pressure of the droplet $p = -\gamma\big(\frac{1}{R_{\mathrm{d},x}} + \frac{1}{R_{\mathrm{d},y}}\big)$, where the negative sign indicates that the pressure acts on the film in the negative z-direction. Note that Eq. S11 is simply the anisotropic Laplace's law in the limit of small slopes.

For the particular case in which $T_{\mathrm{in},x} = T_{\mathrm{in},y}$, we recover the isotropic Laplace's law (small slopes), for which the solution is given by

$$w\,(r) = \frac{pr^2}{4T_{\mathrm{in},x}} + c_0 \ln(r) + c_1 \;, \tag{S12}$$

with $r = \sqrt{x^2 + y^2}$. Since the position of the membrane at $x = y = 0$ must be finite, we find that $c_0 = 0$, whereas $c_1 = w_0$, an arbitrary vertical shift of the system. Therefore, the isotropic solution becomes

$$w\,(x, y) = \frac{p}{4T_{\mathrm{in},x}}\left(x^2 + y^2\right) + w_0 \;, \tag{S13}$$

For the anisotropic case, since ϵ is near 1, we expect that the solution should be very similar to the isotropic case. Thus, we propose

$$w\,(x, y) = Ax^2 + By^2 + Cxy + Dx + Ey + F \;. \tag{S14}$$

In addition, we know that $\partial_x w = \partial_y w = 0$ at $x = y = 0$, which provides the values $D = 0$ and $E = 0$. Once more, at $x = y = 0$ an arbitrary vertical shift of the system w_0 is asigned to the coefficient F. Additionally, we must consider the symmetry conditions: 1) $\partial_x w = 0$ at $x = 0$; 2) $\partial_y w = 0$ at $y = 0$; both implying that $C = 0$.

Therefore, we have

$$w\,(x, y) = Ax^2 + By^2 + w_0 \;. \tag{S15}$$

Plugging this ansatz back into Eq. S11 leads to

$$2T_{\mathrm{in},x}A + 2T_{\mathrm{in},y}B = \gamma\Big(\frac{1}{R_{\mathrm{d},x}} + \frac{1}{R_{\mathrm{d},y}}\Big)\ . \tag{S16}$$

We can also write A and B in terms of $\theta_{\mathrm{b},x}$ and $\theta_{\mathrm{b},y}$. At $x = r_x$, $y = 0$ we have $\partial_x w = 2Ar_x = \tan\theta_{\mathrm{b},x} \approx \theta_{\mathrm{b},x}$. Similarly, $2Br_y \approx \theta_{\mathrm{b},y}$. In addition, a circular cap identity can be used to write $R_{\mathrm{d},x}$ and $R_{\mathrm{d},y}$ in terms of $\theta_{\mathrm{d},x}$ and $\theta_{\mathrm{d},y}$. Thus, Eq S16 becomes

$$\frac{T_{\mathrm{in},x}\theta_{\mathrm{b},x}}{r_x} + \frac{T_{\mathrm{in},y}\theta_{\mathrm{b},y}}{r_y} = \gamma\Big(\frac{\sin\theta_{\mathrm{d},x}}{r_x} + \frac{\sin\theta_{\mathrm{d},y}}{r_y}\Big)\ . \tag{S17}$$

Finally, we arrive at Eq. 4 in the main manuscript

$$\frac{T_{\mathrm{in},x}\theta_{\mathrm{b},x}}{\gamma} + \frac{T_{\mathrm{in},y}\theta_{\mathrm{b},y}}{\gamma\epsilon} = \sin\theta_{\mathrm{d},x} + \frac{1}{\epsilon}\sin\theta_{\mathrm{d},y}\ . \tag{S18}$$

NEUMANN CONSTRUCTION

The three internal angles characterizing the contact line profile are $\pi - \theta_{\mathrm{d}} - \theta_{\mathrm{m}}$, $\theta_{\mathrm{d}} + \theta_{\mathrm{b}}$, and $\pi - \theta_{\mathrm{b}} + \theta_{\mathrm{m}}$. Thus, the internal angles are set by three different linear combinations of the measured angles: $\theta_{\mathrm{d}} + \theta_{\mathrm{m}}$, $\theta_{\mathrm{d}} + \theta_{\mathrm{b}}$, and $\theta_{\mathrm{b}} - \theta_{\mathrm{m}}$. As was done in Ref. [2], one may apply a Neumann construction to attain predictions for these three angle combinations:

$$\cos(\theta_d + \theta_m) = \frac{[T_{out}/\gamma]^2 - [T_{in}/\gamma]^2 + 1}{2\,[T_{out}/\gamma]}, \tag{S19a}$$

$$\cos(\theta_b + \theta_d) = \frac{[T_{out}/\gamma]^2 - [T_{in}/\gamma]^2 - 1}{2\,[T_{in}/\gamma]}, \tag{S19b}$$

$$\cos(\theta_b - \theta_m) = \frac{[T_{out}/\gamma]^2 + [T_{in}/\gamma]^2 - 1}{2\,[T_{out}/\gamma]\,[T_{in}/\gamma]}, \tag{S19c}$$

where $T_{\mathrm{out}} = T_{\mathrm{in}} + \gamma\cos\theta_{\mathrm{Y}}$. These predictions depend only on two parameters: T_{in}/γ and θ_{Y}. Of course, this Neumann construction may be carried out normal to the contact line at any point along the perimeter. Thus, using the value we measure for θ_{Y}, we fit these predictions separately to the measured internal angles in x and in y to find the best fit parameter values of $T_{\mathrm{in},x}/\gamma$ and $T_{\mathrm{in},y}/\gamma$. The best fitted values of $\theta_{\mathrm{d}} + \theta_{\mathrm{m}}$, $\theta_{\mathrm{d}} + \theta_{\mathrm{b}}$, and $\theta_{\mathrm{b}} - \theta_{\mathrm{m}}$ are listed in Table I of the main manuscript.

* dalnoki@mcmaster.ca

[1] N. Nadermann, C.-Y. Hui, and A. Jagota, Proc. Natl. Acad. Sci. U.S.A. **110**, 10541 (2013).
[2] R. D. Schulman and K. Dalnoki-Veress, Phys. Rev. Lett. **115**, 206101 (2015).
[3] S. Timoshenko and J. Goodier, *Theory of Elasticity, 2nd* (McGraw-Hill Book Company, Inc., New York, 1951).
[4] R. Pan and D. Wati, Polym. Composite **17**, 486 (1996).
[5] P. Russo, M. Lavorgna, F. Piscitelli, D. Acierno, and L. Di Maio, Eur. Polym. J. **49**, 379 (2013).
[6] H.-Y. Mi, X. Jing, M. R. Salick, W. C. Crone, X.-F. Peng, and L.-S. Turng, Adv. Polym. Tech. **33** (2014).
[7] D. R. Lide, *CRC Handbook of Chemistry and Physics* (CRC Press, 2004) pp. 6–154.
[8] L. Landau and E. Lifshitz, *Theory of Elasticity, 3rd* (Butterworth-Heinemann, New York, 1986).